· Article · Advances in Polar Science
doi: 10.13679/j.advps.2018.0050 June 2019 Vol. 30 No. 2: 93-105

Surface energy balance on the Antarctic plateau as measured with an automatic weather station during 2014

DING Minghu[1], Anubha AGRAWAL[1*], Petra HEIL[2] & YANG Diyi[1]

[1] State Key Laboratory of Severe Weather and Institute of Polar Meteorology, Chinese Academy of Meteorological Sciences, Beijing 100081, China;
[2] Antarctic Climate & Ecosystems Cooperative Research Centre, Hobart, Tasmania, Australia

Received 30 December 2018; accepted 29 April 2019; published online 30 April 2019

Abstract AWS data during 2014 collected at PANDA-N station, on the East Antarctica Plateau, are analysed. Net Short Wave Radiation (Q_{SWR}), net Long Wave Radiation (Q_{LWR}), sensible (Q_H), latent (Q_L) and subsurface or ground (Q_G) heat fluxes are computed. Annual averages for Q_{SWR}, Q_{LWR}, Q_H, Q_L and Q_G of 19.65, −49.16, 26.40, −0.77 and 3.86 W·m^{-2} were derived based on an albedo value of 0.8. Q_{SWR} and Q_H are the major sources of heat gain to the surface and Q_{LWR} is the major component of heat loss from the surface. An iterative method is used to estimate surface temperature in this paper; surface temperature of snow/ice is gradually increased or decreased, thereby changing longwave radiation, sensible, latent and subsurface heat fluxes, so that the net energy balance becomes zero. Mass loss due to sublimation at PANDA-N station for 2014 is estimated to be 12.18 mm w.e.·a^{-1}; and mass gain due to water vapour deposition is estimated to be 3.58 mm w.e.·a^{-1}. Thus the net mass loss due to sublimation/deposition is 8.6 mm w.e.·a^{-1}. This study computes surface energy fluxes using a model, instead of direct measurements. Also there are missing data especially for wind speed, though 2 m air temperature data is almost continuously available throughout the year. The uncertainties of albedo, wind speed and turbulent fluxes cause the most probable error in monthly values of Q_{LWR}, Q_H, Q_L, Q_G and surface temperature of about ±4%, ±20%, ±50%, ±11% and ±0.74 K respectively.

Keywords energy balance, Antarctica, surface mass loss, CHINARE

Citation: Ding M H, Agrawal A, Heil P, et al. Surface energy balance on the Antarctic plateau as measured with an automatic weather station during 2014. Adv Polar Sci, 2019, 30(2): 93-105, doi:10.13679/j.advps.2018.0050

1 Introduction

Antarctica is the coldest, windiest and driest place on Earth. It has three parts, East Antarctica, West Antarctica and the Antarctic Peninsula. In comparison to mountains of mid-latitude regions, it has very flat topographic relief except in some coastal areas. Due to the threats like sea level rise, changing wind patterns and loss of biodiversity, polar research is given importance in context of global climate research. The Antarctic Ice Sheet's (AIS) role as the major heat sink for Earth's atmospheric circulation makes it a very important region on the globe. However, learning about AIS is still a challenge because of its remote location, inaccessibility, harsh weather conditions and expensive expedition logistics.

The surface energy balance (SEB) of AIS is studied to learn about its climate processes and to monitor the impact of global climate change on the AIS (Van den Broeke et al., 2006; Hoffman et al., 2008; Ma et al., 2011a, 2011b). In particular, information about surface energy fluxes may be used for validation of climate models for Antarctica (King and Connolley, 1997). The Antarctic atmosphere is highly transmissive for solar radiation, especially on the high interior plateau where the atmosphere is thin and concentrations of clouds, water vapour and aerosols are low.

*Corresponding author, E-mail: agrawal.anubha@gmail.com

The ice-sheet has a highly reflective (high albedo) snow surface that limits the absorption of shortwave radiation while effectively losing heat in form of longwave radiation by radiating nearly as a black body (Wiscombe et al., 1980). The atmosphere over Antarctica is cold and lacks water vapour, which limits the gain of downward long-wave radiation (Q_{LWR}). Therefore, the net radiation balance over Antarctica is generally negative on average (e.g. Van den Broeke et al., 2004), yet the SEB differs greatly from the coast to inland Antarctica due to changes in solar zenith angle, cloud condition, surface characteristics, boundary layer etc. For instance, surface characteristics which determine the albedo, are influenced by snow fall, katabatic wind, air temperature and humidity, and can be classified into several types (Scambos et al., 2012). Annual mean albedo values in the range 0.84 to 0.88 for different sites at Antarctica have been reported along with daily mean albedo values as low as 0.78 for a coastal katabatic site (Van den Broeke et al., 2004). Similarly, Zhang et al. (2004) and Fu et al. (2015) reported some inland areas may only absorb 5%–20% of the shortwave radiation in summer.

The SEB over Antarctica has been widely studied (e.g. Schlatter, 1972; Wendler et al., 1988; Bintanja and Van den Broeke, 1995; etc.), such as the solar radiation studies in South Pole (Dutton et al., 1991). Other studies include evaluation of sublimation at Dome A (Ding et al., 2016), the daily cycle and the role of cloud on the energy budget in Dronning Maud Land (DML) (Van den Broeke et al., 2006), and the impact of Foehn winds on the SEB over Larsen C Ice Shelf (King et al., 2017). However, relative to the vast extent of Antarctica, the observations and simulations of energy balance are still very sparse, thus limiting our knowledge on the mechanism of interaction between ice sheet and atmosphere. As a result, regional climate models and earth system models have poor skill in polar regions (IPCC, 2013). Thus, more studies on energy exchange over Antarctic surface snow are still important.

Automatic Weather Stations (AWS) provide continuous surface meteorological data from remote locations with harsh weather conditions, so are one of most important tools for polar studies. PANDA-N AWS is one of several stations set up by the Chinese National Antarctic Research Expedition (CHINARE) in East Antarctica along 77°E longitude. It is located in the interior at a distance of 501 km from the coast at an elevation 2597 m a.s.l. Two important meteorological phenomena are observed in this region – persistent katabatic winds and quasi-permanent surface temperature inversions, and these may lead to heavy sublimation of the snow surface, as noted by Scambos et al. (2012). The area has an average slope of 5.4 m·km^{-1} with a prevailing north-north-westerly aspect. The site is free from any surface melt and the surface snow has a fine grain structure and is well compacted by surface winds. The long-term snow accumulation rate in the region is 67 mm w.e.·a^{-1} (kg·m^{-2}·a^{-1}) (Ding et al., 2011). In this paper, the energy balance at PANDA-N is studied using AWS data. In section 2 we describe the climate and data treatment of the site, in section 3 we describe the experimental setup, followed by results in section 4, comparison with other studies in section 5, discussion in section 6, and a summary in section 7.

2 Site description and data treatment

In 2008 the PANDA-N AWS was installed on the Antarctic plateau at location 73°41′22″S, 76°58′2″E (Figure 1) and at an elevation of 2597 m a.s.l. AWS data from PANDA-N station is collected by the CHINARE as a contribution to the International Trans-Antarctic Scientific Expedition (ITASE). However, initially it did not provide continuous observations. So we use only data during 2014 for this study. The instruments on this AWS are the same as those described in Ma et al. (2011a). The AWS data used in this study are air temperature, air pressure and relative humidity at 2 m height; firn temperature at 0.1, 1, 3 and 3.7 m depths; and wind speed at 1, 2 and 4 m height. Due to power supply limitation, data at the AWS are recorded only at every last minute of the hour, but are treated as hourly data.

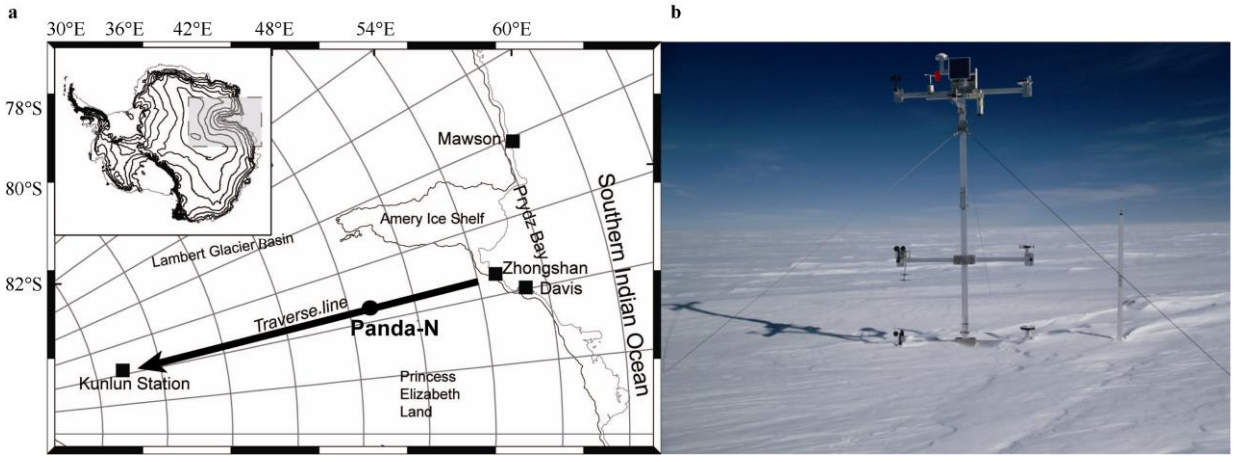

Figure 1 Map of Antarctica showing location (**a**) and photo (**b**) of PANDA-N station.

One issue with the autonomously collected observations is missing data. For example, air temperature at 2 m height was missing only 29 lines due to data relay errors with the ARGOS system out of a total of 8645 data lines for the year 2014. On the other hand, entries for wind speed may be missing during all winter months because of icing/riming of the sensors. For example, for the year 2014, the wind speed is available at one of the three levels for only 2759 lines of a total of 8645 data lines. We replaced any missing wind speed with the most recent actual wind measurement. The resultant average annual wind speed computed for 2 m height at PANDA-N for 2014 is 10 $m \cdot s^{-1}$. From the valid measurements of wind speed, the average wind speed at 1 m height is 1.2 $m \cdot s^{-1}$ lower than the 2 m value and the 4m wind speed is 0.8 $m \cdot s^{-1}$ higher than the 2 m value. We used the same magnitude gradients when wind-speed information was missing at any level. Sensitivity analysis was also made by varying the wind speed by ±1 $m \cdot s^{-1}$; the results of this are depicted by error bars in the respective plots. We find that the effect of wind speed on the SEB is much less than that of albedo. Albedo has been set at 0.8 for this study (referred to *in situ* measurement carried out in Taishan Station in 2011, ~20 km from PANDA-N), and was varied between 0.75 and 0.9 to quantify the effect of albedo on the energy flux values. But sensitivity analysis for an albedo range of 0.75 to 0.85 is shown as error bars in the plots so as to give symmetry around the albedo value of 0.8.

3 Methodology

The SEB (Eq. 1) of the Antarctic plateau is calculated as

$$Q_{SWR} + Q_{LWR+} Q_H + Q_L + Q_G = 0, \quad (1)$$

where, Q_{SWR} = Net shortwave radiation

Q_{LWR} = Net longwave radiation

Q_H = Sensible heat flux

Q_L = Latent heat flux

Q_G = Ground or subsurface heat flux

The surface temperature value is adjusted to achieve a zero net energy residual (Van den Broeke et al., 2005b; Bliss et al., 2011; etc.). At time step 1, the initial value for the snow surface temperature (SST) is taken as the snow temperature at 0.1 m depth as measured by the AWS. For the succeeding timesteps, the surface temperature calculated by iteration from the preceding timestep is taken as the initial value of SST.

3.1 *RH* correction for Vaisala *RH* sensor (RS80-A)

The following relation was proposed by Miloshevich et al. (2001) for correcting the temperature-dependent error of the Vaisala RS80-A humidity sensor.

$$RH = RH' (a_0 + a_1 t + a_2 t^2 + a_3 t^3 + a_4 t^4), \quad (2)$$

where RH is the corrected relative humidity to compensate for the temperature-dependent error in calibration of the Vaisala RS80-A sensor; RH' is the relative humidity value recorded by the humidity sensor; t is air temperature in ℃.

Here, a_0=0.9278, a_1=−5.9662×10^{-3}, a_2=1.578×10^{-4}, a_3=1.8179×10^{-6}, a_4=3.9407×10^{-8}.

This correction in RH value is valid for the temperature range 0℃ to −70℃ (Miloshevich et al., 2001).

3.2 Vapour pressure over water

The saturation vapour pressure over water is computed by the following expression, given by Wexler (1977):

$$\log e_s = h_{-1}/T + h_0 + h_1 \times T + h_2 \times T^2 + h_3 \times T^3 + h_4 \log T, \quad (3)$$

where T is air temperature in K and e_s (Pa) is saturation vapour pressure. The coefficients in equation (3) are:

h_{-1}= −0.58653696×10^4, h_0= 0.2224103300×10^2

h_1= 0.13749042×10^{-1}, h_2= −0.34031775×10^{-4}

h_3= 0.26967687×10^{-7}, and h_4= 0.6918651.

Since the calibration for the Vaisala relative humidity sensor RS80-A is made with respect to the Wexler (1977) formulation of saturation vapour pressure, water vapour pressure (e) at 2 m is calculated by multiplying RH by saturation vapour pressure e_s as calculated above (Moradi, 2015).

$$e = RH \times e_s/100 \quad (4)$$

3.3 Computation of specific heat of ice

Murphy and Koop (2005) derived the molar specific heat C_p ($J \cdot mol^{-1} \cdot K^{-1}$) of ice as a function of the temperature $T > 20$ K.

$$C_p = -2.0572 + 0.14644T + 0.06163T \exp\left\{-\left(\frac{T}{125.1}\right)^2\right\} \quad (5)$$

This expression is used to calculate the thermal energy content of firn when finding the subsurface heat flux. The molar molecular weight of ice is taken as 18.015 $g \cdot mol^{-1}$.

3.4 Computation of cloud-fraction

The cloud fraction n_c is calculated using Eq. (6) as done by Liston and Elder (2006).

$$n_c = 0.832 \exp\left(\frac{RH_{700} - 100}{41.6}\right) \quad (6)$$

Here, RH_{700} is the value of relative humidity at 700 hPa altitude. Since the 2 m air pressure at PANDA-N station averages around 700 hPa, the relative humidity measured by the AWS data is taken as RH_{700}. This value of cloud-fraction is used to calculate the incoming short-wave radiation (Q_{SWR}) and Q_{LWR}.

3.5 Computation of short wave radiation

In this paper, incoming Q_{SWR} is calculated based on the approach given by Liston and Elder (2006).

Firstly the solar altitude angle is calculated as

$$\sin\alpha = \sin L \sin\delta_s + \cos L \cos\delta_s \cos h_s, \quad (7)$$

with the hour angle h_s being a function of the solar time:

$$h_s = (12 \text{ hours} - \text{solartime})\pi/12 \quad (8)$$

Angle of declination is calculated as:

$$\delta_s = 23.45\sin(360°\times(284+N)/365), \quad (9)$$

where N is the Day of Year (DoY).

The solar flux (I_o) outside the atmosphere is calculated using Eq. (10).

$$I_o = S_o\,(1 + 0.0344\cos(360°\mathrm{N}/365)), \quad (10)$$

where, S_o is the solar constant with a value 1367 $\mathrm{W\cdot m^{-2}}$.

The solar radiation is separated into two components: the direct beam radiation and the diffuse solar radiation.

Here, the direct beam radiation (I_p) is computed for the surface which has slope β and azimuth angle or aspect a_w using Eq. (11).

$$I_p = I_s\cos i, \quad (11)$$

where I_s is the radiation observed on a normal surface and i is the angle between the normal to the surface and the direction to the Sun.

And I_s is calculated using Eq. (12).

$$I_s = I_o\tau_b$$
$$\tau_b = \theta(0.6 - 0.2\sin\alpha)(1-n_c), \quad (12)$$

where τ_b is the atmospheric transmittance. And n_c is the cloud fraction calculated by Eq. (6). Liston et al. (1999) used a calibration factor θ equal to 1.2 in the above equation initially given by Burridge and Gadd (1974) to provide a best fit to the observed incoming shortwave radiation at Neumayer Station, Antarctica.

cos$i$ is computed using Eq. (13):

$$\cos i = \sin\delta_s(\sin L\cos\beta - \cos L\sin\beta\cos a_w) + \cos\delta_s\cos h_s$$
$$(\cos L\cos\beta + \sin L\sin\beta\cos a_w) + \cos\delta_s\sin\beta\sin a_w\sin h_s \quad (13)$$

Diffuse radiation (I_d) is calculated using Eq. (14) (Liston and Elder, 1999).

$$I_d = 1.2I_o\sin\alpha(0.3-0.1\sin\alpha)n_c \quad (14)$$

The incoming Q_{SWR} is given by the sum of direct beam radiation I_p and diffuse radiation I_d. Outgoing Q_{SWR} is given by the product of incoming Q_{SWR} and surface albedo. Bian et al. (1993) reported an albedo value of 0.55 for Zhongshan Station, East Antarctica, where there is little snow on the surface; but an albedo of more than 0.8 has been measured for snow covered regions on the Antarctic continental ice sheet (Schlatter, 1972; Bintanja and Van den Broeke, 1995; etc.). Van Lipzig et al. (1999) applied a constant albedo value of 0.8 for surface temperatures below −10℃ in their simulation of the Antarctic atmosphere using a regional atmospheric climate model. Considering that the uppermost 10 m of ice-sheet consists mostly of snow, because the low temperatures in Antarctica make the metamorphosis from snow to ice a slow process (Herron and Langway, 1980), we assume in this study, an albedo value of 0.8. This is consistent with the type of snow near the PANDA-N AWS station which consists of fine grains with an absence of surface melt. As noted earlier, the sensitivity analysis considers albedo values in the range 0.75 to 0.85. Furthermore, as our AWS observations show (Figure 2), the 2 m air temperatures does not reach above −12℃ at any time of year.

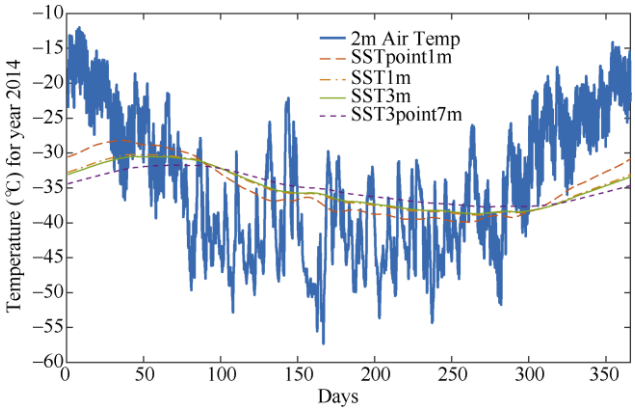

Figure 2 Air temperature at 2 m, SST 0.1 m, SST 3 m and SST 3.7 m for year 2014.

3.6 Computation of longwave radiation

Liston and Elder (2006) suggested use of an expression for incoming longwave radiation proposed by Iziomon et al. (2003), which is suitable for surfaces extending across a range of altitudes. The meteorological model (Micromet) described by Liston and Elder (2006) has been applied for several Antarctic studies, e.g. Liston et al. (1999, 2000), and Liston and Winther (2005). Downward longwave radiation (LWR ↓) and upward longwave radiation (LWR ↑) are calculated using Eqs. (15) and (16).

$$\mathrm{LWR}\downarrow = \varepsilon\sigma T_a^4 \quad (15)$$

$$\mathrm{LWR}\uparrow = \sigma T_s^4 \quad (16)$$

$$\varepsilon = k[1+\mathrm{Zn}_c^2]\left[1 - X\exp\left(-Y\frac{\sigma}{T_a}\right)\right] \quad (17)$$

Here, ε is emissivity of the atmosphere; T_a is 2 m air temperature in K and e is 2 m water Vapour pressure in Pa; k=1.083; σ is Stefan Boltzmann's constant (=5.667×10^{-8} $\mathrm{W\cdot m^{-2}\cdot K^{-4}}$); T_s is SST (K). It is assumed that surface emissivity for snow and ice equals one. The coefficients X, Y and Z depend on elevation according to

$$X = 0.35 + (z-200)\left(\frac{0.51-0.35}{3000-200}\right)$$
$$Y = 0.100 + (z-200)\left(\frac{0.130-0.100}{3000-200}\right) \quad (18)$$
$$Z = 0.224 + (z-200)\left(\frac{1.1-0.224}{3000-200}\right)$$

Where coefficients X, Y and Z are defined for elevation in the range $200 \leqslant z \leqslant 3000$ m.

3.7 Computation of turbulent fluxes

Following Hock (2005), sensible (Q_H) and latent (Q_L) heat fluxes may be calculated using Eqs. (19) and (20):

$$Q_H = \rho_a C_p C_H \bar{u}(\theta_z - \theta_s) \quad (19)$$

$$Q_L = \rho_a L_s C_L \bar{u}(q_z - q_s) = \rho_a L_s C_L \bar{u}(e_z - e_s)\frac{0.622}{p}, \quad (20)$$

where, ρ_a is the density of air, C_p is specific heat of air (1.005×10^3 J·kg^{-1}·K^{-1}), C_H is the coefficient for heat (1.27×10^{-3}; Ma, 2009), C_L is the coefficient for vapour pressure (1.29×10^{-3}; Ma, 2009), L_s is the latent heat of sublimation, q_z and q_s are the specific humidity (dimensionless) at height z (2 m) and the snow surface, respectively, θ_z and θ_s are potential temperatures (K) at height z (2 m) and the snow surface respectively, p is the 2 m air pressure (hPa) and e_z and e_s are vapour pressures (hPa) at height 2m and the snow surface respectively. Vapour pressure e_z at a height z is computed as in Eq. (4), while vapour pressure e_s at the snow surface is calculated by Eq. (21). With SST T in K, the saturation vapour pressure e_s (Pa) over ice is given by Murphy and Koop (2005):

$$e_s = \exp\left(9.550426 - \frac{5723.265}{T} + 3.53068\ln(T) - 0.00728332T\right); T > 110K \quad (21)$$

To calculate vapour pressure e_s at the surface of snow/ice, RH is taken as 100% at the snow surface. The latent heat of sublimation for ice in J·mol^{-1} given by Murphy and Koop (2005) and shown in Eq. (22) is used, with a molar mass of 18.015 g·mol^{-1} for water.

$$L_s = 46782.5 + 35.8925T - 0.07414T^2 + 541.5\exp\left\{-\left(\frac{T}{273.115}\right)^2\right\}; T > 30K \quad (22)$$

Potential temperature is a function of temperature and pressure. It is computed from Eq. (23)

$$\theta = T\left(\frac{p_o}{p}\right)^{0.286}, \quad (23)$$

where, T is air temperature (K), p (bar) is air pressure and p_o is 1 bar pressure.

3.8 Bulk aerodynamic method of calculating turbulent fluxes

The methodology used in this work for calculating Q_H and Q_L is similar to the one described in Van den Broeke et al. (2005b). Stability corrections to the semi-logarithmic profiles used are the same as proposed by Holtstag and de Bruin (1988) for stable conditions, while the functions of Dyer (1974) are used for unstable conditions. The surface roughness length for momentum is calculated using wind speed data at 1 and 4 m heights with the value restricted between 1×10^{-6} m and 1×10^{-3} m. Here roughness lengths for air temperature and specific humidity are calculated using expressions from Andreas (1987). Turbulent temperature and humidity scales are calculated using potential temperature and specific humidity at 2 m height and the snow surface.

3.9 Computation of mass loss

At PANDA-N station there is no mass loss by melting. To solve the mass balance, we apply an iterative approach. Similar to Van den Broeke et al. (2005b) and Bliss et al. (2011), the net energy balance or residual of energy balance equation, i.e. the sum of terms on LHS of Eq. (1) is computed for each AWS data line. The mass loss or gain is computed using Eq. (24):

$$\text{Mass loss/gain} = \frac{Q_L \Delta t}{L_s}\ \text{mm w.e.}, \quad (24)$$

where L_S is latent heat of sublimation calculated by Eq. (22), and Δt is the time increment. Mass is lost by sublimation when Q_L is negative and gained by deposition of water vapour when Q_L is positive.

3.10 Subsurface/ground flux

Shortwave radiation penetration is neglected as the fine grain dry snow at PANDA-N station tends to be opaque to Q_{SWR} as it scatters back the high frequency component of Q_{SWR}, while absorbing most of the infra-red component in the top 0.01 m thickness of snow (Brandt and Warren, 1993).

The subsurface flux is calculated as the change in thermal energy of the snow pack to 10 m depth (Munneke et al., 2009). The snow densities for the first 2 m depth are given in Table 1, while beyond 2 m depth density is assumed to linearly increase to 587 kg·m^{-3} at a depth of 20 m. This snow density of 587 kg·m^{-3} at 20 m depth is based on *in situ* measurements obtained at DT05, 35 km north of PANDA-N station. The one-dimensional heat conduction equation is explicitly solved using a time increment of 1 s and a space increment of 0.01 m with the temperature at the snow surface as per the current iteration value and under the assumption of an insulated boundary at 10 m depth. The vertical temperature profile is initialized for every time-step by linear interpolation using the AWS-derived snow/firn temperature at 0.1 m, 1 m, 3 m and 3.7 m depths. The initial temperature at 10 m depth is assumed to be 0.16℃ smaller than that at 3.7 m depth; this assumption is based on the measurements by an AWS station Eagle, at a distance of 305 km from PANDA-N, where the annual average snow temperatures at 3 m and 10 m depths differ by 0.16℃. Since the firn temperature is initialised every hour, the thermal energy change of only the first few meters of firn is sufficient for accurate calculation of the subsurface heat flux.

Table 1 Snow density measured by volume-weight method for the first 2 m depth at PANDA-N station, in January 2011

Depth/cm	0–10	10–20	30	40	50	60	70	80	90	100	110	130	150	160	180	200
Density/(kg·m^{-3})	373	514	495	448	434	423	412	449	419	502	430	461	413	454	418	423

The thermal conductivity of snow is assumed to be a function of density. Sturm et al. (1997) suggested an expression for thermal conductivity for snow at temperature below or near −14.6℃ to be:

$$k = 0.138 - 1.01\times10^{-3}\rho + 3.233\times10^{-6}\rho^2, \quad (25)$$

where ρ is snow density in kg·m^{-3}and k is thermal conductivity in W·m^{-2}·K^{-1}. Because of wind packing, Antarctic snow is relatively dense with a large thermal conductivity in the range 0.2–0.3 W·K^{-1}·m^{-1}. Many studies (e.g. Liston et al., 1999) have used the same expression in their analyses for Antarctica.

4 Results and analysis

4.1 Weather station data

4.1.1 Air temperature

In 2014 the 2 m air temperature stayed below 0℃ throughout the year (Figure 2). Annual average, and the minimum and maximum 2 m air temperatures observed were −34.5℃, −57.32℃ and −12.0℃, respectively.

4.1.2 Relative humidity, vapour pressure and wind speed

Relative humidity at the study region varies from 18%–100% with an average value of 76.2% for 2014 (Figure 3). Average annual cloud-fraction computed using this relative humidity value is 0.48.

The average annual 2 m wind speed observed was 10.36 m·s^{-1} for 2014 (Figure 3). Katabatic winds persist year-round at the site, averaging 8–10 m·s^{-1} over the year, with a summer average of 8.7 m·s^{-1} and a winter average of 11.5 m·s^{-1}.

Average vapour pressure is 0.26 hPa. Vapour pressure at 2 m height ranges from 0.011 to 1.57 hPa for 2014 (Figure 4).

4.1.3 Snow surface temperature (SST)

The computed snow-surface temperature stays below 0℃ throughout the year. Average, minimum and maximum SSTs are −37.11℃, −57.33℃ and −14.74℃ for 2014.

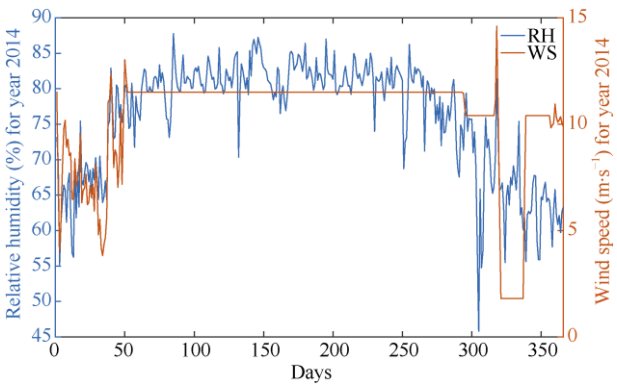

Figure 3 Relative humidity and wind speed at 2 m for year 2014.

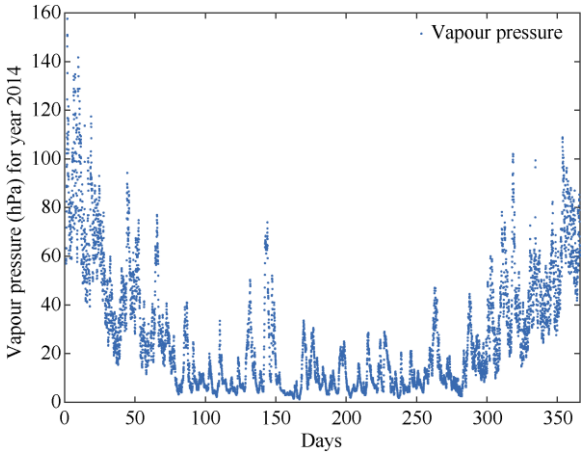

Figure 4 Vapour pressure at 2 m for year 2014.

Average, minimum and maximum daily average snow/firn temperatures, at 0.1 m depth, are −35.12℃, −39.9℃ and −28.18℃ respectively for the year 2014.

The iterative method estimates the surface temperature by enforcing energy balance at the AWS location. For 2014, monthly mean values of air temperature at 2 m height, snow temperature at 0.1 m depth and computed SST are shown in Figure 5. Throughout the year the average 2 m air temperature is higher than surface temperature, thus causing a positive sensible heat flux. The average monthly gradient between the 2 m air temperature and SST varies between 1.29℃ and 5.22℃ with an average annual difference of 2.56℃.

On average, SST is higher than the snow temperature at 0.1 m depth in austral summer, but lower in winter when longwave radiation cools the surface of the ice sheet and the ground heat flux is positive, i.e. heat flows from below to the surface. The average monthly difference between SST and snow temperature at 0.1 m depth ranges from −10.85℃ to 7.12℃ with an average annual difference of −1.99℃ making the net annual subsurface heat flux to the surface positive.

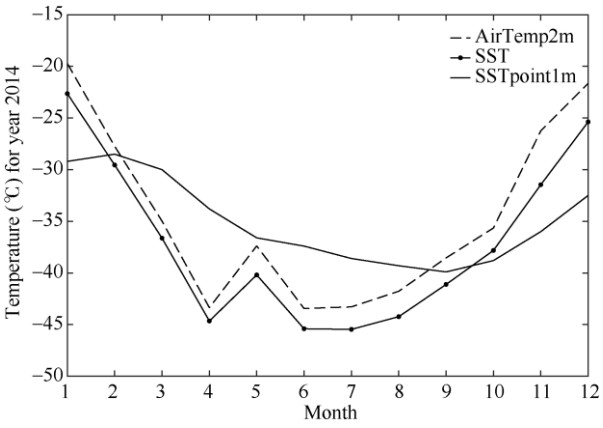

Figure 5 Monthly average air temperature at 2 m, SST and SST

0.1 m for year 2014.

4.2 Energy balance components

Figure 6 shows the mean values of the energy fluxes for 2014 from the iterative method. The monthly mean Q_{SWR}, ranges from 0 to 54.37 W·m^{-2}; Q_{LWR} from −38.91 to −69.14 W·m^{-2}; Q_H from 15.62 to 40.58 W·m^{-2}; Q_L from −4.76 to 0.87 W·m^{-2}; and Q_G from −15.93 to 22.85 W·m^{-2}. These values are calculated based on an albedo of 0.8.

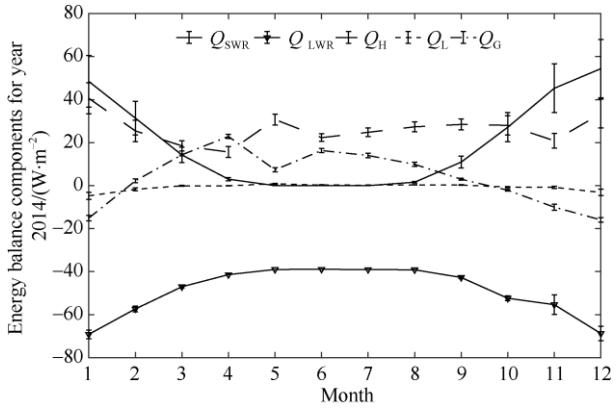

Figure 6 Monthly mean surface energy fluxes for year 2014 with error bars showing most probable uncertainty for variations in albedo (0.8±0.05), wind speed (±1 m·s^{-1}) and surface roughness value.

4.2.1 Shortwave radiation

Daily Q_{SWR} ranges from 0 to 92 W·m^{-2} with an average annual value of 19.65 W·m^{-2}. Maximum Q_{SWR} values are observed during December with a monthly average of 54.37 W·m^{-2}. The mean for summer months January, February, November and December (JFND) is 44.86 W·m^{-2}. The average annual atmospheric transmittance for direct beam radiation is computed to be 0.368.

The albedo strongly influences the net shortwave radiation flux. More solar energy input to the ice-sheet and thereby an increase in its surface temperature is seen with any decrease in albedo. Increase of surface temperature results in greater longwave radiation loss and an increase of the latent heat flux by increasing the saturation vapour pressure at the surface. The annual mean of Q_{SWR} varies from 24.6 to 9.8 W·m^{-2} as albedo varies from 0.75 to 0. 9.

4.2.2 Longwave radiation

The largest monthly derived mean for Q_{LWR} is for January at −69.14 W·m^{-2}, while the annual mean Q_{LWR} is −49.16 W·m^{-2}. As albedo varies from 0.75 to 0.9, annual mean Q_{LWR} varies from −50.3 to −46.8 W·m^{-2}. Average annual emissivity of the atmosphere is 0.695.

4.2.3 Net radiation

Annual mean net radiation, the sum of Q_{SWR} and Q_{LWR}, is −29.51 W·m^{-2} for an albedo of 0.8. Net radiation ranges from a monthly mean −10.09 W·m^{-2} in November to an average of −39.03 W·m^{-2} over the winter months April to August. The ice-sheet continuously loses radiative heat throughout the year.

4.2.4 Latent heat flux

The annual average value of Q_L is −0.77 W·m^{-2}, with a maximum monthly average of −4.76 W·m^{-2} in January. As albedo varies from 0.75 to 0.9, the annual mean value of Q_L varies from −1.23 to 0.01 W·m^{-2}.

4.2.5 Sensible heat flux

The annual average Q_H is 26.4 W·m^{-2}. The maximum Q_H is observed during summer months (JFND) with an average of 30.1 W·m^{-2}. The average Q_H during the winter months April to August is 24.15 W·m^{-2}. The maximum monthly mean is found during January with a value of 40.58 W·m^{-2}. Most studies report maximum Q_H during winter (e.g. Hoffman et al., 2008). The explanation for this peculiarity is that the increase in surface temperature at PANDA-N station during austral summer is less than the increase in ambient air temperature, causing a large temperature difference and consequently higher sensible heat flux during January and December. This is due to the situation of PANDA-N station where relatively high wind speeds are seen along with large shortwave radiation flux in months of January and December.

The average monthly value of Q_H is positive all year round, meaning that the surface is gaining heat from the atmosphere by sensible heat transfer, thus acting as a heat sink throughout the year.

As albedo varies from 0.75 to 0.9, the annual mean value of Q_H varies from 23.8 to 31.6 W·m^{-2}, with an average January maximum reaching 54.8 W·m^{-2} for an albedo of 0.9.

4.2.6 Subsurface or ground heat flux

The annual mean Q_G is 3.86 W·m^{-2}, implying that there is net annual heat loss from the ice-sheet at PANDA-N station. The subsurface heat flux is positive in austral winter and negative in austral summer, varying from −15.93 W·m^{-2} in December to 22.85 W·m^{-2} in April. As albedo varies from 0.75 to 0.9, the annual mean Q_G varies from 3.2 to 5.4 W·m^{-2}.

4.2.7 Mass loss

The annual mass loss by sublimation during 2014 computed from Q_L is 12.18 mm w.e.·a^{-1} (kg·m^{-2}·a^{-1}). The annual mass gain by vapour deposition during the same period is 3.58 mm w.e.·a^{-1}. Thus, the average annual net mass loss by sublimation/deposition is 8.6 mm w.e.·a^{-1}. From the results it is seen that Q_{SWR} and Q_H are the main sources of heat gain at the surface, and Q_{LWR} is the main component of heat loss, i.e. about 99%. The remainder is latent heat flux which is responsible for mass-loss by sublimation.

As albedo varies from 0.75 to 0.9, net annual mass loss

varies from 13.7 mm w.e.·a^{-1} for albedo of 0.75 to a net annual mass gain of 0.1 mm w.e.·a^{-1} for albedo of 0.9.

4.3 Diurnal cycle

Figure 7 shows the diurnal cycle of a typical summer day (DoY 2, 2014). The 2 m air-temperature varies between −13.9℃ and −19.3℃ with corresponding surface temperatures between −16.9℃ and −22.6℃, and 2 m wind speeds between 5.2 m·s^{-1} and 3.7 m·s^{-1}.

Average net radiative flux for DoY 2, 2014 is −12.5 W·m^{-2} showing that the snow surface loses radiative heat during a typical summer day at PANDA-N. Sensible heat transfer for DoY 2, 2014 varies between 4.7 and 63.8 W·m^{-2} with corresponding 2 m wind speeds between 2.2 and 10.5 m·s^{-1}, and net radiative flux between 9.9 and −39.7 W·m^{-2}; the corresponding temperature inversions between 2 m air temperature and surface snow temperature are 6.1℃ and 3.2℃. Thus, the observations of low value of sensible heat flux and positive value of radiant heat flux at wind speed of 2.2 m·s^{-1} imply that low wind speeds at about or below 2 m·s^{-1} reduce the sensible heat flux drastically yielding much lower SSTs to meet SEB. Average sensible heat flux, temperature inversion and 2 m wind speed for DoY 2, 2014 are 37.0 W·m^{-2}, 4.4℃ and 6.5 m·s^{-1}, respectively which shows that vigorous turbulent exchanges accompanied by intense winds cause net cooling of the katabatic layer; persistent katabatic flow is maintained by a steady supply of negatively buoyant air down the slope. Also Q_G varies between −31.7 and 1.2 W·m^{-2}, with an average value of −22.3 W·m^{-2} during the day, showing substantial heat loss due to ground flux during a typical summer day.

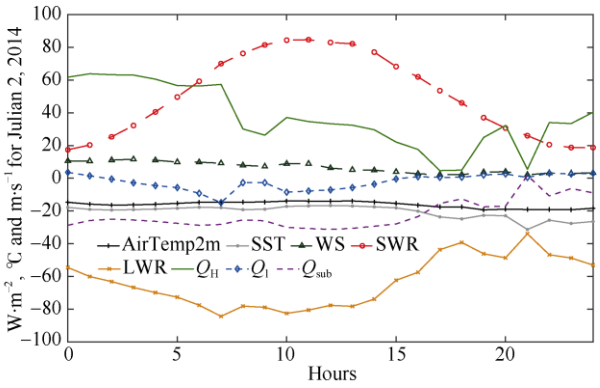

Figure 7 Surface energy fluxes, air temperature at 2 m, SST and 2 m wind speed for DoY 2 for year 2014.

Figure 8 shows diurnal cycle of a typical winter day (DoY 153, 2014). Compared to DoY 2, energy terms for DoY 153 show much less daily variation; net Q_{LWR} varies between −39.0 W·m^{-2} and −41.7 W·m^{-2}; Q_H varies between 16.5 W·m^{-2} and 21.7 W·m^{-2} and Q_G varies between 17.7 W·m^{-2} and 24.0 W·m^{-2} with corresponding 2 m air temperatures between −46.7°C and −43.2℃. This indicates fluctuation in air temperature causes variations in the components of the surface energy flux. Mean wind speed at 2 m height is assumed to be 11.5 m·s^{-1} as actual wind speed data is missing for DoY 153.

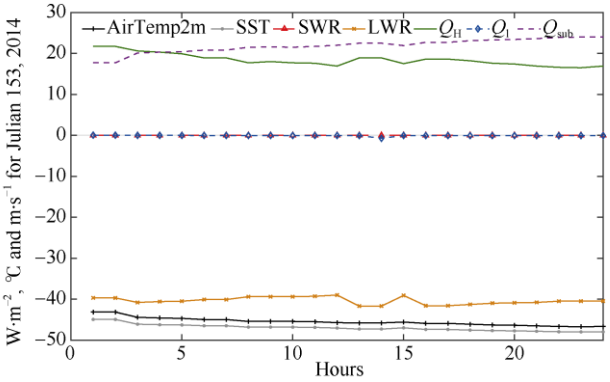

Figure 8 Surface energy fluxes, air temperature at 2 m and SST for DoY 153 for year 2014 with 2 m wind speed assumed to be 11.5 m·s^{-1}.

4.4 Sensitivity analysis

In this paper, the energy balance at PANDA-N station is studied using AWS data. The present study computes Q_{SWR} and Q_{LWR} based on sub-components proposed for use over the ice sheet by Liston and Elder (2006). Turbulent fluxes are calculated by the bulk aerodynamic method using wind, air temperature and humidity measurements. The determination of turbulent fluxes, effect of cloud fraction on radiation flux, and surface albedo are commonly identified as the most prominent uncertainties. In this work, there is a problem of missing observations of wind speed during winter, which causes uncertainty especially for the turbulent flux terms.

Results have been derived for an albedo of 0.8 with possible variation in the range 0.75 to 0.9. But sensitivity analysis for an albedo range of 0.75 to 0.85 is shown as error bars in Figure 6 so as to give symmetry around the albedo value of 0.8. The SST plays an important role in the estimates of turbulent fluxes. In this work SST is assessed by an iterative procedure seeking to minimize the error in net energy balance. The iterative procedure helps to reduce the effect of uncertainties of various terms of energy balance equation and obtaining the correct net energy residual of zero.

A 25% change in net Q_{SWR} flux causes changes of the mean monthly surface flux values during January in Q_{LWR}, Q_H, Q_L and Q_G, of the order of 3%, 17%, 33% and 9% respectively; the resultant change in surface temperature is 0.56 K. A change in wind speed by 1 m·s^{-1} causes changes for the mean monthly surface flux values during January in Q_{LWR}, Q_H, Q_L and Q_G of the order of 2%, 7%, 20% and 5% respectively; the resultant change in surface temperature is 0.34 K. In this study, the surface roughness length for momentum is calculated using wind speeds at 1 m and 4 m heights, though its value is restricted between 1×10^{-6} m and

1×10^{-3} m. If surface roughness for momentum is fixed at 1×10^{-4} m, changes for the mean monthly values in Q_{LWR}, Q_H, Q_L and Q_G and surface temperature during January are of the order of 2%, 8%, 32%, 5% and 0.34 K respectively; while changes for the mean annual values in Q_{LWR}, Q_H, Q_L and Q_G and surface temperature are of the order of 1.1%, 4.7%, 1.1%, 13.2% and 0.25 K respectively.

The uncertainties of albedo, wind speed and turbulent fluxes cause maximum change for the month of January. The most probable error in monthly values of Q_{LWR}, Q_H, Q_L, Q_G and surface temperature due to all these uncertainties is about 4%, 20%, 50%, 11% and 0.74 K respectively. The latent heat flux is small at PANDA-N because of the low surface air temperature, so the importance of uncertainty in its value is relatively low. The sensible heat flux is large, but uncertainty in its monthly mean is only 20%, which is reasonable considering the large uncertainties assumed in albedo, wind speed and surface roughness length. This shows that the calculated magnitude of surface energy terms is robust. The error bars in Figure 6 show uncertainty in the different energy terms.

5 Comparison of the PANDA-N SEB with other regions

The increase in surface temperature in austral summer results in greater longwave radiation loss and an increase in latent heat flux, due to increase in saturation vapour pressure at the surface. Also, the sensible heat flux is seen to increase in austral summer because of the larger difference between air temperature and SST along with increased wind speeds. This behaviour is peculiar to PANDA-N station, as the net radiative, latent and subsurface heat fluxes are all negative during January and December, and are compensated by sensible heat transfer which is highest for these months. Average daily net radiative flux is negative throughout the year at PANDA-N.

Mass loss by sublimation occurs predominantly in austral summer. Larger sublimation mass loss occurs in summer months due to the higher surface temperature because of heat gain from Q_{SWR}. Annual mass loss due to sublimation for 2014 was 12.2 mm w. e., while annual mass gain by deposition was 3.6 mm w. e. Overall mass loss by sublimation is much less at PANDA-N station as it is located at a high altitude with a lower value of specific humidity due to its low surface air temperature. For example, Van den Broeke et al. (2009) reported an annual mean value of sublimation mass loss at the Antarctic coastal station Neumayer as 40 mm w.e. for the period 1995–2007 and an average deposition of 14 mm w. e.

In a summer study (DoYs 296–51, 1998–2001), Van den Broeke et al. (2006) reported average cloud cover of 33% for the Antarctic interior region compared to 54% for the coastal region. For all sky condition, net Q_{SWR} was reported as 53 $W\cdot m^{-2}$ and 56 $W\cdot m^{-2}$ for AWS6 and AWS9 respectively; whereas it was 68 $W\cdot m^{-2}$ and 65 $W\cdot m^{-2}$ respectively for clear-sky conditions. AWS6 is located in the inland region of DML, East Antarctica at an altitude of 1160 m a. s. l. and has a surface slope of 15 $m\cdot km^{-1}$ and mean 10 m wind speed of 6.6 $m\cdot s^{-1}$. AWS9 is located in the polar plateau region in DML at 2892 m a. s. l. and has a surface slope of 1.3 $m\cdot km^{-1}$ and mean 10 m wind speed of 5.0 $m\cdot s^{-1}$. Summertime mean net Q_{SWR} for January, February, November and December (JFND) for PANDA-N at an albedo of 0.8 is 45 $W\cdot m^{-2}$, which is 20 % lower than the all-sky value of 56 $W\cdot m^{-2}$ for AWS9. Annual mean cloud-fraction is calculated as 0.48 using relative humidity data at PANDA-N station.

Net Q_{LWR} for the DoYs 296–51, 1998–2001, was reported to be −55 and −53 $W\cdot m^{-2}$ for all-sky condition for AWS6 and AWS9 respectively, with corresponding values of −78 $W\cdot m^{-2}$ and −64 $W\cdot m^{-2}$ for clear sky conditions. Monthly mean of net Q_{LWR} for months of JFND for PANDA-N station is −63 $W\cdot m^{-2}$ which is within 20 % of the net Q_{LWR} value of −53 $W\cdot m^{-2}$ for AWS9.

Under clear sky conditions in summertime at AWS9, Van den Broeke et al. (2006) reported that for all-sky conditions, Q_G reached 20 $W\cdot m^{-2}$ in a day with values ranging from 20 to −23 $W\cdot m^{-2}$; they found that Q_G is the most effective SEB component to compensate net radiative transfer on sub-daily timescales, especially under clear-sky conditions. In this present study, monthly mean Q_G ranges from −15.9 $W\cdot m^{-2}$ in December to 22.9 $W\cdot m^{-2}$ in April in 2014. Also, in the present study for 2014 DoY 2, a typical summer day, Q_G varies from −31.2 to 1.7 $W\cdot m^{-2}$.

For AWS6, Van den Broeke et al. (2005b) reported a 1998–2001 annual mean Q_H of 24.2 $W\cdot m^{-2}$; monthly mean Q_H during winter was between 20–40 $W\cdot m^{-2}$; mean Q_H for January and December were 8 and 6 $W\cdot m^{-2}$ respectively. For PANDA-N, Q_H for January and December, 2014 were 40.6 and 33.5 $W\cdot m^{-2}$ respectively and the annual mean Q_H value was 26.4 $W\cdot m^{-2}$ with the monthly mean ranging between 15.62 and 40.58 $W\cdot m^{-2}$. Both the stations show positive sensible heat flux values throughout the year as both are in katabatic drainage zones.

Liston et al. (1999) reported annual mean Q_{SWR}, Q_{LWR}, Q_H, Q_L and Q_G values as 29.3, −17.9, 3.6, −19.3 and 4.3 $W\cdot m^{-2}$ respectively for a snow surface at Jutulgryta, in the coastal area of DML (150 m a.s.l.). The derived mean annual net Q_{SWR} in the present study is 19.7 $W\cdot m^{-2}$ for an albedo of 0.8, whereas an albedo of 0.75 was assumed by Liston et al. (1999). A Q_G value of 4.3 $W\cdot m^{-2}$ is comparable with the value of 3.9 $W\cdot m^{-2}$ obtained for PANDA-N, though values of Q_H and Q_L are quite different.

Bintanja and Van den Broeke (1995) presented SEB results for other locations in DML, Antarctica. The results for Site 5, at an altitude of 1150 m a.s.l., at a distance of 290 km from the coast, are similar to the results from PANDA-N in this study. They presented results for 28 December 1992 – 10 February 1993; the mean 2 m temperature and SST for their study were −11.4 and

−13.3℃ and mean 6 m wind speed was 5.8 m·s^{-1}; Q_{SWR}, Q_{LWR}, Q_H, Q_L and Q_G were 63.1, −58.5, 18.5, −22.1 and −1.0 W·m^{-2} respectively. The mean diurnal range of Q_H was from 40 to −5 W·m^{-2}. For January 2014, PANDA-N has mean values of Q_{SWR}, Q_{LWR}, Q_H, Q_L and Q_G of 48.43, −69.14, 40.58, −4.76 and −15.1 W·m^{-2} respectively; mean 2 m air temperature and SST for January of −19.72℃ and −22.64℃ and the 2 m mean wind speed was 7.5 m·s^{-1}. Q_H values for DoY 2 ranged between 63.8 and 4.6 W·m^{-2}. The present study and the study by Bintanja and Van den Broeke (1995) show large Q_H values in the month of January because both locations have high wind speeds and significant temperature inversions.

Similarly, a study for December 28, 1997 to February 2, 1998 by Bintanja (2000) found for a location called Site 7, at an altitude of 2100 m a. s. l., that steeper slopes and stronger winds did induce a large downward directed sensible heat flux. He called the surface heat budget at that site 'peculiar' as in the literature he found no other region except for the South Pole with similar characteristics, i.e. negative net radiation accompanied by a positive turbulent flux in summer. In this study, the mean 2 m temperature and SST were −17.8℃ and −19.7℃; mean 2 m wind speed was 5.7 m·s^{-1}; mean 2 m relative humidity and specific humidity were 68.1% and 0.79 g·kg^{-1}; Q_{SWR}, Q_{LWR}, Q_H, Q_L and Q_G were 50.1, −63.5, 20.4, −6.2 and −0.7 W·m^{-2} respectively; and the mean diurnal range of Q_H was from 10 to 28 W·m^{-2}. Corresponding heat flux values for PANDA-N for January 2014 are 48.43, −69.14, 40.58, −4.76 and −15.1 W·m^{-2} respectively. Similarity in the two results is because of metrological commonalities of high wind speeds and sustained temperature inversions, along with similar altitude (2100 vs 2597 m a.s.l.). Bintanja (2000) also remarked that for the Site 7, solar heating is unable to sufficiently raise the surface temperature to create a well-mixed boundary layer, in contrast to the usual observation (e.g. Fortuin and Oerlemans, 1992; Ding et al., 2016) of near-neutral and unstable conditions in summer daytime in the Antarctic interior.

At Kohnen Station, on the high Antarctic plateau at an altitude of 2892 m a. s. l., Van As et al. (2005a, 2005b) reported annual mean 2 m air temperature of −43.2°C with a range from −15℃ to −70℃ and annual mean wind speed of 4.3 m·s^{-1}; annual mean net Q_{SWR} for 1998–2001 was 23 W·m^{-2}, compared to 19.65 W·m^{-2} for PANDA-N , and net Q_{LWR} was −30 W·m^{-2}, compared to −49.16 W·m^{-2} for PANDA-N. The higher loss due to Q_{LWR} at PANDA-N than at Kohnen, can be explained by relatively higher surface temperature at PANDA-N, caused by larger wind speeds that resulted in higher sensible heat transfer from the atmosphere to the snow surface. A short-term experiment at Kohnen from 8 January 2002 to 9 February 2002 showed that albedo varied between 0.83 and 0.92 with a mean value of 0.86 and that variations were due to changes in cloud amount and solar elevation (Van As et al., 2005a). Daily mean Q_G values ranged from −8 to 7 W·m^{-2}, with a daily variation between −16 and 22 W·m^{-2}; and like the turbulent heat fluxes, the subsurface heat flux opposed the mean radiative flux. At PANDA-N station, for 2014 DoY 2, Q_G varied between −31.2 and 1.7 W·m^{-2}.

At a near-coastal ice shelf station, Neumayer (40 m a.s.l.) during 1997–2007, where 2 m air temperature was −16℃; surface temperature was −17℃; relative humidity was 92%; albedo was ~0.85; and 10 m wind speed was 9.1 m·s^{-1}; Van den Broeke et al. (2009) calculated the SEB components. Net Q_{SWR}, net Q_{LW}, Q_H, Q_L, Q_G and Q_M were 18.5, −29.0, 12.7, −2.3, 0.5 and −0.5 W·m^{-2} respectively. For PANDA-N, the present study reports annual mean Q_{SWR}, Q_{LWR}, Q_H, Q_L and Q_G values of 19.65, −48.43, 26.4, −0.77 and 3.86 W·m^{-2} respectively. Net Q_{SWR} at PANDA-N is quite close to the value at Neumayer, while net Q_{LWR} is much larger than the value at Neumayer. PANDA-N station has higher altitude (2597 vs 40 m a.s.l.), therefore it has lower air temperature (−34.5℃), resulting in much lower incoming Q_{LWR}. Also, Q_L is lower at PANDA-N because of lower specific humidity resulting from the cold surface air temperature.

The results from this present PANDA-N study are comparable to those from previous studies. Some differences can be explained by the geographical peculiarities of PANDA-N. Most of the studies compared involved direct measurements of Q_{SWR} and Q_{LWR}, while the present study computes Q_{SWR} and Q_{LWR} using expressions suggested by Liston and Elder (2006). Some of the studies mentioned for comparison use the bulk aerodynamic method as well as direct eddy correlation measurements to estimate the turbulent sensible and latent heat fluxes, while the present work is based solely on the bulk aerodynamic method. For example, Van den Broeke et al. (2006) derived surface momentum length from on-site eddy correlation measurements and, assuming it to be constant in time, they calculated turbulent fluxes by the bulk aerodynamic method. They also reported a close agreement between the fluxes calculated by the bulk aerodynamic method and the fluxes from eddy correlation measurements reported by Bintanja (2000) and Van As et al. (2005a) for two summer experiments. In summary, we suggest that the methodology used here for calculating energy balance terms for PANDA-N station is robust.

6 Discussion

The last section compared the results of this study with other studies to confirm the robustness of the methodology used. This section discusses the PANDA-N surface energy fluxes compared with those at other sites over Antarctica to explain any peculiarity in results in terms of geographical characteristics of the PANDA-N station region.

Van den Broeke (2005a) presented a comparison of surface energy fluxes (for 1998–2001) calculated from

AWS data at four locations in DML, East Antarctica. These were AWS4 (34 m a.s.l., coastal ice shelf), AWS5 (363 m a.s.l., coastal katabatic wind zone), AWS6 (1160 m a.s.l., inland katabatic wind zone) and AWS9 (2892 m a.s.l., polar plateau). Surfaces were almost flat for AWS4 (< 1 m·km^{-1}) and AWS9 (1.3 m·km^{-1}), while surfaces at AWS5 and AWS6 had slopes of 13.5 and 15 m·km^{-1} respectively. Annual mean 10 m wind speeds for AWS4, AWS5, AWS6 and AWS9 were 5.7, 7.8, 7.7 and 4.8 m·s^{-1} respectively, and mean annual 2 m air temperatures were −18.8, −16.3, −20.5 and −43℃ respectively. In comparison, PANDA-N AWS is located in the interior at a distance of 501 km from coast, at an elevation of 2597 m a.s.l. and the area has an average slope of 5.4 m·km^{-1}. It is in a katabatic wind zone with average annual 2 m wind speed of about 10 m·s^{-1} and mean annual 2 m air temperature of −34.5℃ for 2014. PANDA-N has a relatively higher mean wind speed than the other two katabatic wind zone sites despite a smaller slope. Parish (1991) noted that the inland wind speed maximum occurs in areas of modest terrain slopes of about 5 m·km^{-1} rather than the steepest terrain slopes. Also PANDA-N has a much higher mean annual 2 m air temperature than that at AWS9 which cannot be explained alone from the adiabatic lapse rate. However, an increase of 5–10℃ can be explained by katabatic vertical mixing of air (Van den Broeke, 2005b); stronger winds bring down warmer air from the inversion-layer to the surface (Hudson and Brandt, 2005, Vihma et al., 2011). Higher air temperature and wind speed result in higher sensible heat flux in the katabatic wind zone. Annual mean sensible heat fluxes at AWS4, AWS5, AWS6 and AWS9 were 7.6, 21.7, 24.1 and 8.0 W·m^{-2} respectively, while it is 26.4 W·m^{-2} for PANDA-N station. A distinguishing feature of PANDA-N station is summer-time higher mean values for sensible heat flux than winter values, e.g. the monthly mean for January is 40.6 W·m^{-2} and that for May is 30.7 W·m^{-2}. The results presented by Van den Broeke et al. (2005a) however, show higher values for the inland katabatic zone (AWS6) in winter than summer, e.g. monthly mean for January is 8 W·m^{-2} and that for June is 38 W·m^{-2}. The reason for this peculiarity at PANDA-N is its higher altitude (2597 m a.s.l.) combined with being a katabatic zone. The higher altitude contributes significantly in causing a deficit in radiation budget throughout the year because of lower incoming Long Wave Radiation (LWR). Summers have, in addition, higher outward LWR and greater loss due to ground flux because of higher surface temperature. Negative radiation budget, negative ground flux and negative latent heat flux need to be compensated by larger sensible heat flux facilitated by high wind speed and a large temperature inversion near the surface.

The magnitude of latent heat flux is maximum in the coastal katabatic zone, followed by the inland katabatic zone (AWS6), coastal ice shelf, PANDA-N station and the polar plateau region (AWS9) in decreasing order. The polar plateau region has minimum air temperature and specific humidity leading to much lower sublimation rates.

Annual mean net radiation is negative at all sites, but with highest magnitude (−29.4 W·m^{-2}) at PANDA-N station followed by AWS6, AWS5, AWS9 and AWS4 in decreasing order. Also, only PANDA-N station shows negative monthly mean radiation in summer months, while other locations show positive net radiation for summer months of January and December. The inland katabatic region (AWS6) has −22.2 W·m^{-2} annual mean radiation while the coastal ice shelf region (AWS4) has −7.6 W·m^{-2}: This can be attributed to much higher sensible heat flux at AWS6 resulting in higher SST and consequently higher outward LWR**.** Monthly mean ground flux is −15 W·m^{-2} at PANDA-N station for summer months of January and December. In summer months, high sensible heat flux makes the SST significantly higher than subsurface temperatures, causing a relatively large negative mean monthly ground flux at PANDA-N. PANDA-N station shows relatively larger magnitudes of mean monthly ground flux throughout the year compared to the other stations. Monthly mean sensible heat flux is highest at PANDA-N in January because of negative mean monthly net radiative flux, latent heat flux and ground flux. High wind speed is important in generating turbulent heat exchange as seen for AWS stations in katabatic wind zones.

7 Conclusions

Surface meteorological observations at PANDA-N station during 2014 are analysed and used for energy flux calculations. This study computes surface energy fluxes using a model, instead of direct measurements. The study is limited by missing wind data, especially in winter months. In this work, SST is assessed by an iterative procedure that seeks to minimise the error in net energy balance. The iterative procedure helps to reduce the uncertainties of various terms of the energy balance equation. It is seen that the methodology used is robust and results from PANDA-N station are comparable with those from other studies while some peculiarities of the results can be explained in terms of the geographical characteristics of PANDA-N station.

The annual average energy balance components computed using the iterative method for 2014 for Q_{SWR}, Q_{LWR}, Q_H, Q_L and Q_G are 19.65, −49.16, 26.40, −0.77 and 3.86 W·m^{-2} respectively. The region is characterised by negative net radiation flux and positive sensible heat flux throughout the year. High wind speed and a large temperature inversion near the surface result in the large downward sensible heat flux. In summer months, the high sensible heat flux makes the SST significantly higher than subsurface temperatures, causing a relatively large negative ground flux. PANDA-N station has low specific humidity leading to low sublimation rates. Loss of latent heat is important only in summer months when SSTs are relatively higher. In winter, the snow surface gains heat from both ground flux and sensible heat flux. But the average sensible heat flux is higher in summer months than in winter for

PANDA-N station, something not seen at other sites. This peculiarity can be explained by the high altitude (2597 m a.s.l.) of PANDA-N station along with strong winds (average annual 2 m wind speed ~ 10 $m \cdot s^{-1}$). These geographical characteristics create a situation of negative radiation budget, negative ground flux and negative latent heat flux for the summer months that need to be compensated by large sensible heat flux which is facilitated by high wind speed and large temperature inversion near the snow surface. The SEB estimates from this study can be useful to validate output from climate models for Antarctica (King and Connolley, 1997; Bintanja, 2000).

Acknowledgements This work was funded by the Ministry of Science and Technology of the People's Republic of China (MOST, Grant no. 2016YFC1400303), the Strategic Priority Research Program of Chinese Academy of Sciences (Grant no. XDA20100300) and the Basic Scientific Research and Operation Foundation of CAMS (Grant no. 2018Z001). Especially, we sincerely thank Editors Ian Allison and Michiel Van den Broeke for their detailed suggestions.

References

Andreas E L. 1987. A theory for the scalar roughness and the scalar transfer coefficients over snow and sea ice. Bound Lay Meteorol, 38: 159-184.

Bian L G, Jia P Q, Lu L H, et al. 1993. Observational study of annual variations of the surface energy balance components at Zhongshan Station of Antarctica in 1990. Sci China Ser B, 36(8): 976-987.

Bintanja R. 2000. Surface heat budget of Antarctic snow and blue ice: Interpretation of spatial and temporal variability. J Geophys Res, 105(D19): 24387-24407.

Bintanja R, Van den Broeke M. 1995. The surface energy budget of Antarctic snow and blue ice. J Appl Meteorol, 34: 902-926.

Bliss A K, Cuffey K M, Kavanaugh J L. 2011. Sublimation and surface energy budget of Taylor Glacier, Antarctica. J Glaciol, 57(204): 684-696.

Brandt R E, Warren S G. 1993. Solar-heating rates and temperature profiles in Antarctic snow and ice. J Glaciol, 39(131): 99-110.

Burridge D M, Gadd A J. 1974. The Meteorological Office operational 10 level numerical weather prediction model (December 1974), U.K. Met. Office Technical Notes 12 and 48, 57.

Ding M, Xiao C, Li Y, et al. 2011. Spatial variability of surface mass balance along a traverse route from Zhongshan Station to Dome A, Antarctica. J Glaciol, 57(204): 658-666.

Ding M H, Xiao C D, Yang Y D, et al. 2016. Re-assessment of recent (2008-13) surface mass balance over Dome Argus, Antarctica. Polar Res, 35, 26133, http://dx.doi.org/10.3402/polar.v35.26133.

Dutton E G, Stone R S, Nelson D W, et al. 1991. Recent interannual variations in solar radiation, cloudiness, and surface temperature at the south pole. J Climate, 4(8): 848-858.

Dyer A. 1974. A review of flux-profile relationships. Bound Lay Meteorol, 7: 363-372.

Fortuin J P F, Oerlemans J. 1992. An atmospheric model for simulating the mass balance and temperature on the Antarctic ice sheet. Z Gletscherkd Glazialgeol, 26(1): 31-56.

Fu L, Bian L G, Xiao C D, et al. 2015. An observational study of the radiation balance on eastern Antarctic Plateau. Acta Meteorol Sin, 73(1): 211-219.

Herron M M, Langway Jr C C. 1980. Firn densification: An empirical model. J Glaciol, 25: 373-385.

Hock R. 2005. Glacier melt: a review of processes and their modeling. Prog Phys Geog, 29(3): 362-391.

Hoffmann M J, Fountain A G, Liston G E. 2008. Surface energy balance and melt thresholds over 11 years at Taylor glacier, Antarctica. J Geophys Res, 113(F04014): 1-12.

Holtstag A A M, de Bruin H A R. 1998. Applied modelling of the night-time surface energy balance over land. J Appl Meteorol, 27: 689-704.

Hudson S R, Brandt R E. 2005. A look at the surface-based temperature inversion on the Antarctic Plateau. J Climate, 18: 1673-1696.

IPCC. 2013. Climate Change 2013: The Physical Science Basis. Contribution of Working Group I to the Fifth Assessment Report of the Intergovernmental Panel on Climate Change. Stocker T F, D Qin, G K Plattner, M Tignor, S K Allen, J Boschung, A Nauels, Y Xia, V Bex and P M Midgley (eds.). Cambridge University Press, Cambridge, United Kingdom and New York, NY, USA.

Iziomon M G, Mayer H, Matzarakis A. 2003. Downward atmospheric longwave irradiance under clear and cloudy skies: Measurement and parametrization. J Atmos Sol-Terr Phy, 65: 1107-1116.

King J C, Connolley W M. 1997. Validation of the surface energy balance over the Antarctic ice sheets in the U.K. meteorological office unified climate model. J Climate, 10: 1273-1287.

King J C, Kirchgaessner A, Bevan S, et al. 2017. The impact of Föhn winds on surface energy balance during the 2010-2011 melt season over Larsen C Ice Shelf, Antarctica. J Geophys Res: Atmospheres, 122(22): 12062-12076.

Liston G E, Elder K. 2006. A meteorological distribution system for high resolution terrestrial modelling (MicroMet). J Hydrometeorol, 7: 217-234.

Liston G E, Winther J G. 2005. Antarctic surface and subsurface snow and ice melt fluxes. J Climate, 18: 1469-1481.

Liston G E, Winther J G, Bruland O, et al. 1999. Below-surface ice melt on the coastal Antarctic ice sheet. J Glaciol, 45(150): 273-285.

Liston G E, Winther J G, Bruland O, et al. 2000. Snow and blue-ice distribution patterns on the coastal Antarctic ice sheet. Antarct Sci, 12(1): 69-79.

Ma Y F. 2009. Characteristic parameters of near surface layer of the traverse route from Zhongshan station to Dome-A, East Antarcitca. Master's Thesis (in Chinese), Beijing, Chinese Academy of Meteorological Sciences.

Ma Y F, Bian L B, Xiao C D. 2011a. Impacts of snow accumulation on air temperature measured by automatic weather stations on the Antarctic ice sheet. Adv Polar Sci, 22(1): 17-24, doi: 10.3724/SP.J.1085.2011.00017.

Ma Y F, Bian L B, Xiao C D, et al. 2011b. Characteristics of near surface turbulent parameters along the traverse route from Zhongshan station to Dome A, East Antarctica. Chin J Geophys, 54(8): 1960-1971.

Miloshevich L M, Vomel H, Paukkunen A, et al. 2001. Characterization and correction of relative humidity measurements from Vaisala RS80-A radiosondes at cold temperatures. J Atmos Ocean Tech, 18: 135-156.

Moradi I. 2015. Enhancing tropospheric humidity data records from satellite microwave and radiosonde sensors. Phd Thesis, Department of Earth and Space Sciences, Chalmers University of Technology, Goteberg, Sweden.

Munneke P K, Van den Broeke M R, Reijmer C H, et al. 2009. The role of radiation penetration in the energy budget of the snowpack at Summit, Greenland. The Cryosphere, 3: 155-165.

Murphy D M, Koop T. 2005. Review of the vapour pressure of ice and supercooled water for atmospheric applications. Q J Roy Meteor Soc, 131(608): 1539-1565.

Parish T R 1991. The katabatic wind regime at Adelie Land, Antarctica. Int J Climatol, 11: 97-107.

Scambos T A, Frezzotti M, Haran T, et al. 2012. Extent of low-accumulation 'wind glaze' areas on the east Antarctic plateau: implications for continental ice mass balance. J Glaciol, 58(210): 633-647.

Schlatter T W. 1972. The local surface energy balance and subsurface temperature regime in Antarctica. J Appl Meteorol, 11: 1048-1062.

Sturm M, Holmgren J, Köing M, et al. 1997. The thermal conductivity of seasonal snow. J Glaciol, 43(143): 26-41.

Van As D, Van den Broeke M, Reijmer C, et al. 2005a. The summer surface energy balance of the high Antarctic plateau. Bound Lay Meteorol, 115: 289-317.

Van As D, Van den Broeke M, Van de Wal R. 2005b. Daily cycle of the surface layer and energy balance on the High Antarctic Plateau. Antarct Sci, 17(1): 1-13.

Van den Broeke M, König-Langlo G, Picard G, et al. 2009. Surface energy balance, melt and sublimation at Neumayer Station, East Antarctica, Antarct Sci, 22(1): 87-96, doi: 10.1017/S0954102009990538.

Van den Broeke M R, Reijmer C, Van de Wal R. 2004. Surface radiation balance in Antarctica as measured with automatic weather stations. J Geophys Res, 109, D09103.

Van den Broeke M, Reijmer C, Van As D, et al. 2005a. Seasonal cycles of Antarctic surface energy balance from automatic weather stations. Ann Glaciol, 41: 131-139.

Van den Broeke M, Van As D, Reijmer C, et al. 2005b. Sensible heat exchange at the antarctic snow surface: a study with automatic weather stations. Int J Climatol, 25(8): 1081-1101.

Van den Broeke M, Reijmer C, Van As D, et al. 2006. Daily cycle of the surface energy balance in Antarctica and the influence of clouds. Int J Climatol, 26: 1587-1605.

Van Lipzig N P M, Meijgaard E V, Oerlemans J. 1999. Evaluation of a regional atmospheric model using measurements of surface heat exchange processes from a site in Antarctica. Mon Weather Rev, 127: 1994-2011.

Vihma T, Tuovinen E, Savijärvi H. 2011. Interaction of katabatic winds and near-surface temperatures in the Antarctic. J Geophys Res, 116, D21119, doi: 10.1029/2010JD014917.

Wendler G, Ishikawa N, Kodama Y. 1988. The heat balance of the icy slope of Adelie Land, Eastern Antarctica. J Appl Meteorol, 27: 52-65.

Wexler A. 1977. Vapour pressure formulation for ice. J Res Natl Bureau Standards, 81, A(1): 5-20.

Wiscombe W J, Warren S G. 1980. A model for the spectral albedo of snow: 1: Pure snow. J Atmos Sci, 37(12): 2712-2733.

Zhang Y C. 2004. Calculation of radiative fluxes from the surface to top of atmosphere based on ISCCP and other global data sets: refinements of the radiative transfer model and the input data. J Geophys Res, 109(D19), D19105.